SigMix: Decoding Superimposed Signals for IoT

Wen Cui, *Student Member, IEEE*, Chen Liu, Hamed Mosavat-Jahromi, *Student Member, IEEE*, and Lin Cai, *Fellow, IEEE*

***Abstract*—The growth of Internet of Things (IoT) is anticipated to accelerate in the coming years. However, the wireless spectrum is insufficient to support the ever-growing IoT applications. A promising solution is to allow concurrent wireless transmissions and decode the superimposed signal. To make this solution practical for IoT systems, dynamic channel conditions and hardware imperfections are the key practical challenges, but not yet be addressed in the past work, leading to a low decoding performance. In this article, we introduce SigMix, aiming to deal with the practical challenges by proposing a solution to decode the superimposed signal, and eventually boost the spectrum efficiency. To this end, we first derive a theoretical expression that reveals the close relationship between phase shifts among concurrently transmitted signals and the error probability in decoding the superimposed signal. Then, based on the theoretical expression, we propose a rotation code and an adaptive decoding scheme to largely reduce the decoding error probability. Extensive experiments have shown that the median bit-error-rate of our scheme is one-order lower than the state-of-the-art.**

***Index Terms*—Spectrum efficiency, superimposed signals, wireless communication.**

I. Introduction

INTERNET of Things (IoT) will experience explosive growth in the coming years. It is estimated that approximately 15 billion IoT devices will be deployed [1] and the global market value will reach $1.2 trillion in 2022 [2]. Since the wireless spectrum is at a premium, wireless communication systems encounter a grand challenge to support the massive number of IoT connections. Traditionally, to improve the spectrum efficiency, dedicated wireless resources, such as the time/frequency/space/code domain resource, are scheduled (orthogonal) to each wireless user. However, two users may compete for the same resource for transmissions due to the well-known hidden terminal problem [3], [4] or scheduling failures [5]. In this case, a collision would happen and none of the transmissions can be decoded by these orthogonal access technologies, which in turn affects the wireless spectrum efficiency and network throughput negatively.

To boost the spectrum efficiency with severe resource competition, a promising solution is to allow concurrent wireless transmissions and decode the superimposed signals via careful signal processing. Recently, there are two main approaches in decoding the superimposed signal: 1) successive interference cancellation (SIC), a major technology in nonorthogonal multiple access (NOMA) [6], [7] and 2) physical-layer network coding (PNC) [8], [9]. Specifically, SIC relies on infrastructure and channel feedback for strict power control, which may not be desirable for low-cost IoT devices and may cause extra delay. PNC requires a relay node as a helper, which is incompatible to the general scenario where the superimposed signal is required to be decoded directly at the receiver.

In this article, we aim to deal with the challenge with a solution to decode the superimposed signal without power control or any helper. Using the toy example shown in Fig. 1(a), when two binary phase-shift keying (BPSK) modulated signals arrive at a receiver concurrently, four possible combinations (i.e., four constellation points) exist in the IQ domain, representing "11," "10," "01," and "00." With noises, the received signals become four clusters centered at the four points. Following a maximum-likelihood scheme, the superimposed signal can be decoded, assuming that the clusters are distinguishable [10].

However, in practice, as shown in Fig. 1(b), the constellation points may be so close to each other that their clusters are indistinguishable, resulting in a high probability of decoding error. This situation occurs due to the signal variation caused by dynamic channel conditions and hardware imperfections, and it will be exacerbated in the IoT systems. Consequently, although the idea is simple, no such system exists due to these practical difficulties.

This article presents SigMix, the first practical system that can decode the superimposed signals under dynamic channel conditions and hardware imperfections for IoT systems. Given the popularity of orthogonal frequency-division multiplexing (OFDM), SigMix is applied to OFDM systems with multiple subcarriers. In a nutshell, SigMix is based on the observation that, for superimposed signals, the distance between constellation points is largely determined by the phase shift between the transmitted signals. Therefore, we can manipulate the phase shift to achieve a desirable decoding performance. It is nontrivial to realize SigMix due to the following challenges.

1) A guideline is missing for manipulating the phase shift.

Manuscript received October 10, 2019; revised December 17, 2019; accepted December 29, 2019. Date of publication January 7, 2020; date of current version April 14, 2020. This work was supported in part by the Natural Sciences and Engineering Research Council of Canada, in part by the Canada Foundation for Innovation, in part by the B.C. Knowledge Development Fund, in part by the China Scholarship Council, and in part by the Natural Science Foundation of China under Grant 61828301. *(Corresponding author: Lin Cai.)*

Wen Cui, Hamed Mosavat-Jahromi, and Lin Cai are with the Department of Electrical and Computer Engineering, University of Victoria, Victoria, BC V8P 5C2, Canada (e-mail: wencui@uvic.ca; hamedmosavat@uvic.ca; cai@ece.uvic.ca).

Chen Liu is with the Department of Information Science and Technology, Northwest University, Xi'an 710127, China, and also with the Department of Electrical and Computer Engineering, University of Victoria, Victoria, BC V8P 5C2, Canada (e-mail: liuchen@nwu.edu.cn).

Digital Object Identifier 10.1109/JIOT.2020.2964598

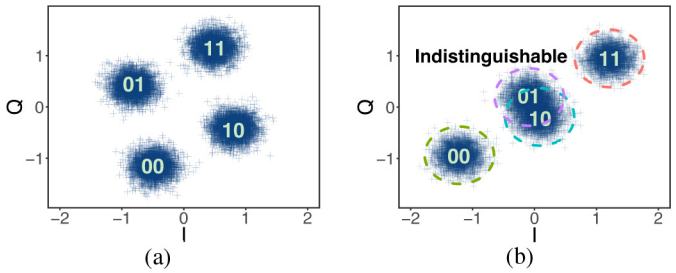

Fig. 1. Superimposed signals in the IQ domain. (a) Example A. (b) Example B.

2) Due to dynamic channel conditions and hardware imperfections in IoT systems, the signal variations are unpredictable, making it difficult to maintain the optimal phase shift at the receiver.
3) The superimposed signal decoder encounters serious signal variations. In the OFDM systems, the channel conditions of different subcarriers are different [11], [12]. Furthermore, the hardware imperfections introduce the carrier frequency offset (CFO), the sampling frequency offset (SFO), and the sample timing offset (STO) to the signal. These offsets cannot be easily compensated for superimposed signals. Moreover, these offsets exacerbate the differences among subcarriers, resulting in a poor decoding performance.

To deal with the first challenge, we derive an exact bit-error-rate (BER) expression to model the relationship between the phase shift and the decoding error probability. This BER expression provides us an important guideline to manipulate the phase shift to achieve a high decoding performance, in terms of a low decoding error rate.

To deal with the second challenge, we propose a rotation code that enables SigMix to transmit two copies of the signal to achieve a substantial diversity gain. Specifically, we only rotate one copy of the signal and keep the other copy as the original one. By doing so, we can eliminate the signal variation caused by dynamic channel conditions and hardware imperfections. Thus, the receiver can eventually decode the superimposed signal with the best phase shift. To further obtain the optimal rotating angle, we propose a searching scheme based on our theoretical analysis.

To deal with the last challenge, we propose an adaptive decoding scheme considering both the subcarriers' differences and the three offsets. With this design, SigMix decodes the superimposed signal based on the behaviors of each subcarrier, which can handle the signal variations well and achieve a high decoding performance.

To the best of our knowledge, this article is the first to present a practical decoding approach for the superimposed signals in the presence of dynamic channel conditions and hardware imperfections. Note that SigMix can be an enabler for many promising wireless technologies requiring the decoding of superimposed signals, such as NOMA and PNC. SigMix is presented in the context of OFDM, hence, the basic idea can be extended to a wide range of application scenarios, e.g., LTE, IEEE 802.11a/g/n/p, etc.

Contributions: This article makes the following contributions.

1) It is the first to reveal the relationship between the phase shift of the concurrent signals and the decoding BER by leveraging Craig's analytical model. As a result, we use this relationship as a guideline in manipulating the phase shift so that a lower BER can be obtained.
2) It presents the first practical approach for decoding superimposed signals through a rotation-code-based diversity transmission and an adaptive decoding scheme. Our approach can achieve a high decoding performance regardless of the practical challenges in IoT systems, i.e., dynamic channel conditions and hardware imperfections, substantially enhancing the decoding ability in practice.
3) It demonstrates a practical system on a software-defined radio-based platform and evaluates its performance across various scenarios. The extensive experimental results illustrate that SigMix obtains a one-order lower median BER than the state-of-the-art system.

The remainder of this article is organized as follows. Section II discusses the related work. Section III presents the background knowledge. Section IV introduces the design of SigMix. Section V discusses several important practical issues. Section VI presents the evaluation results and further discussions. We conclude this article in Section VIII.

II. Related Work

Prior work falls into the following four categories.

1) *SIC:* To decode the superimposed signal, SIC requires strict power control to guarantee that one signal has much higher power than the others. With the power differences, they can decode one of the signals first while treating others as noise, and then cancel it out to decode the rest. Eventually, all signals can be decoded separately by repeating this procedure, e.g., BASIC [13] and CoReCast [7]. As a major NOMA technology, SIC is promising for future cellular networks [14]–[18]. However, it relies on infrastructure and channel feedback for the strict power control, which may not be desirable for low-cost IoT devices and may cause extra delay [19], [20]. In contrast, SigMix does not need power control and extra channel feedback, therefore, we can support a wider range of IoT applications.
2) *PNC:* The superimposed signals can also be decoded with the help of a relay node[1] [26], [27]. This idea has been moved from theory to practice by the implementation of PNC [8], [21] and analog network coding (ANC) [22]. Follow-up work extended these systems to be more robust [9], [21], scalable [28]–[30], and achieving higher throughput (e.g., BiPass [23] employed the high-cost full-duplex devices). However, these works were designed for relay networks, making them incompatible to decode the superimposed signals without the help of other nodes. Some recent work proposed to decode the superimposed signals directly at the receiver

[1]In relay networks, two end nodes transmit signals concurrently so signals are superimposed at the relay, and then the relay node broadcasts this superimposed signal back the end nodes. Each end node can decode the signal transmitted from the other end node by canceling out its own signal.

TABLE I
COMPARISON OF RELATED WORK IN HANDLING SUPERIMPOSED SIGNALS

Properties	BASIC [13]	CoReCast [7]	PNC [8], [21]	ANC [22]	BiPass [23]	NetScatter [24]	Hubble [25]	SigMix
Data Rate	$\sim$ Mbps	$\sim$ Mbps	$\sim$ Mbps	$\sim$ Kbps	$\sim$ Mbps	$\sim$ Kbps	$\sim$ Kbps	$\sim$ Mbps
Synchronization Level	Packet	Symbol	Symbol	Packet	Packet	Symbol	Symbol	Symbol
Power Control	Yes	Yes	No	No	No	No	No	No
Interference Decoding	Yes	Yes	No	No	No	Yes	Yes	Yes
Modulation Scheme	OFDM	OFDM	OFDM	MSK	OFDM	CSS	On-Off Key	OFDM
Device Cost	Low	High	Low	Low	High	Low	Low	Low
Error Control	Retran.	Retran.	Coding	Retran.	Retran.	Retran.	Coding	Coding

without any helper. Strong assumptions, such as a perfect channel measurement and a stable environment, are required [31]. The perfect channel measurement can only be obtained by dedicated hardware [31], [32], such as cellular base stations, which can hardly be achieved in the low-cost IoT devices [33]. Instead of a perfect channel measurement, researchers proposed to decode the superimposed signals with retransmissions to reduce the decoding error [7], [10], [34]–[36]. But the retransmission may introduce a long delay. Different from the previous work, SigMix can decode the superimposed signal directly at the receiver without any helper. Furthermore, with an adaptive decoding scheme, SigMix can achieve a high decoding performance (i.e., a lower BER) without relying on the perfect channel measurement nor retransmissions.

3) *Superimposed Signals in Low Data Rate Systems:* Decoding superimposed signal has also been widely adopted in other IoT techniques with a low data rate, such as LoRa [37] (e.g., NetScatter [24]) and RFID [19], [38], [39] (e.g., Hubble [25]) and ZigBee [40]. These approaches are promising for low data rate applications, such as weather reports, that only generate a few packets per minute [41]. However, applications with general data rate requirements, for example, farm monitoring [42], are beyond the capability of these approaches. Indeed, decoding the superimposed signals in general data rate technology supported by OFDM (e.g., Wi-Fi)[2] is much challenging than that in the low data rate technology. On the one hand, the signals are more vulnerable to dynamic channel conditions when the data rate becomes higher [32]. On the other hand, a low data rate technology can leverage some notable features, such as the frequency diversity in LoRa [24], the signal state transitions in RFID [25], or the oversampling in ZigBee [40], to separate the superimposed signal, but these features are inapplicable to the general data rate technology, e.g., OFDM. In contrast to these low data rate technologies, SigMix aims to be applied to general data rate systems, such as OFDM.

4) *Multiple-Input–Multiple-Output (MIMO) Systems and Superimposed Signals:* Decoding the superimposed signal using MIMO technologies has attracted many research interests [32], [43], where signals are transmitted concurrently via multiple antennas co-located within one transmitter, but the MIMO solution may be too expensive for low-cost IoT devices. Furthermore, SigMix is not only applicable for low-cost IoT devices but also compatible with the MIMO systems, especially for distributed MIMO applications [44], [45].

[2]Cisco predicts that Wi-Fi will be one of the dominating technologies for the coming wireless data traffic in IoT [1].

As a summary, a detailed comparison between SigMix and the existing work is shown in Table I.

III. PRELIMINARY

A. Superimposed Signal's Representation

When different transmitters transmit to the same receiver concurrently, the receiver will receive a superimposed signal, i.e., a combination of these transmitted signals over the air. In the frequency domain, without loss of generality, we define the received superimposed signal as Y, the channel matrix as $\mathbf{H}$, the transmitted signals as $\mathbf{X}$, and the additive white Gaussian noise as N. Then, we have

$$Y = \boldsymbol{HX} + N. \tag{1}$$

Here, m elements in $\mathbf{X}$ represent m transmitters, and $\mathbf{H}$ represents the signal variation caused by both the channel and hardware. It is worth noting that the concurrent transmissions fall into the category of symbol-level synchronization that can be achieved by the existing implementations [10], [46]. More details will be discussed in Section V.

For decoding the superimposed signal, we convert the above frequency-domain representation to the IQ domain. We start by considering the mix of two BPSK modulated signals for simplicity. When a receiver receives two signals simultaneously, if without noises, there are four possible combinations (i.e., four constellation points) exist in the IQ domain, representing 11, 10, 01, and 00. Given random noises, the received signals will be distributed in clusters centered at these constellation points (see Fig. 1).

B. Craig's Analytical Model

1) Craig's Polar Coordinate: For superimposed signals, the locations of the constellation points are irregular, making the decoding error probability difficult to calculate. Craig's polar coordinate [47] can simplify the decoding error probability calculation. As shown in Fig. 2(a), in the constellation map, one of the channel coefficients (e.g., H_1) is co-located with the I-axis when using Craig's polar coordinate. The phase shift between transmitted signals is defined as ϕ (i.e., the angle between H_1 and H_2). Four black dots represent four constellation points. The whole area is partitioned into four decision regions, i.e., regions A_1, A_2, A_3, and A_4, namely, a Voronoi diagram. The boundaries of the decision regions are shown as

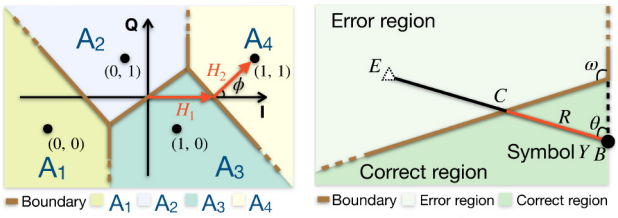

Fig. 2. Craig's analytical model. (a) Craig's polar coordinate. (b) Unit shape.

the brown lines. Here, regions A_1 and A_4 are symmetrical with the origin. Similarly, regions A_2 and A_3 are also symmetrical. Note that both H_1 and H_2 determine the locations of the constellation points and the corresponding decision region. Following a maximum-likelihood decoding, any received symbol[3] in each region will be decoded to the symbol represented by the constellation point in that region.

2) Decoding Error Probability: When a received symbol is incorrectly located to other decision regions, an error happens. We use Craig's analytical model to calculate the probability of errors.

Considering a general case shown in Fig. 2(b), Y is a received symbol and it can be correctly decoded only if it is located in the correct decision region, say location B. Due to the effect of the Gaussian noise, Y may be drifted away to a location, say E, in an error region. Here, the error region is a wedge area bounded by two rays (i.e., two boundaries). The correct location B is outside the error region and on the extension line of one boundary ray. For simplicity, we define the above-mentioned wedge area together with location B as a *unit shape*. The Craig angle ω is defined as the angle between two boundaries. Segment EB crosses the decision boundary at point C, and the distance from B to C is R. Then, according to the theory in [48], the probability that a received symbol is incorrectly located to the error region can be defined as the decoding error probability P, given by

$$P = \int_0^{\omega} d\theta \int_L^{\infty} p(r,\theta)dr \tag{2}$$

where $p(r,\theta)$ is the polar form of the bivariate Gaussian distribution function, and r is the length of segment EB. After a series of transformations, (2) can be written as

$$P = \frac{1}{2\pi}\int_0^{\omega} \exp\left(-\frac{R^2(\theta)}{2\sigma^2}\right)d\theta \tag{3}$$

where $2\sigma^2$ refers to the noise density and $R(\theta)$ means that the distance R is a function of θ. Fortunately, (3) only contains elementary functions, which can largely simplify the calculation process. We refer the readers who are interested in (3) to [48] for more details. Note that (3) can only calculate the decoding error probability under the unit shape.

IV. SigMix Design

In this section, we first derive the BER expression to quantify the decoding performance and identify the factors affecting the decoding performance. With the guideline from the detailed quantitative analysis, we then propose a diversity transmission scheme with a rotation code and design an adaptive decoding scheme accordingly, aiming for a better decoding performance in terms of a lower BER.

[3]A superimposed signal consists of many symbols. When two BPSK modulation signals are superimposed, each symbol carries two bits from two transmitters.

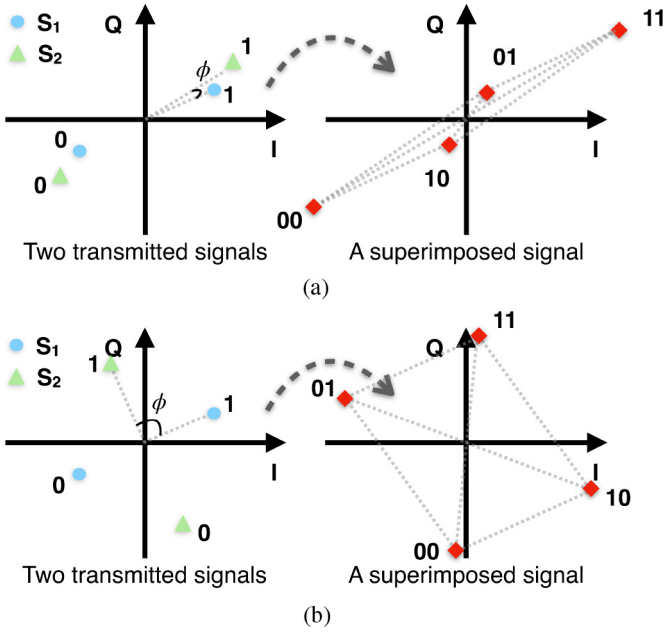

Fig. 3. Phase shift versus constellation points. (a) $\phi = 10°$. (b) $\phi = 90°$.

A. BER Analysis

1) Derivation of the BER Expression: As shown in Fig. 3(a), two transmitters, S_1 and S_2, transmit signals concurrently. We first consider perfect channels where no signal variation exists. When the phase shift ϕ between two transmitted signals is 10°, two constellation points (10 and 01) are very close to each other, making it difficult to decode successfully. However, when the phase shift is changed[4] to 90°, as shown in Fig. 3(b), the four constellation points are far away from each other, making it easy to decode.

The distances between the constellation points in the IQ domain are largely determined by the phase shift. Therefore, we need to model the relationship between the phase shift and the decoding error rate. In the following, we derive the exact BER expression given both the amplitude- and phase-related information, rather than coarse error probability bounds obtained in [34], [36], and [49] that are determined by the signal-to-noise ratio (SNR) only.

We use Craig's polar coordinate to derive the exact BER expression. The decoding error probability, P, can be written as

$$P(e) = \sum_{i=1}^{4} P(e|A_i)P(A_i) \tag{4}$$

where $P(A_i)$ is the probability of transmitted symbols corresponding to the constellation point in decision region A_i, and

[4]Theoretically, we can also change the signal amplitude to change the distances between the constellation points. However, manipulating the signal amplitude may be impractical due to the low-cost IoT devices, and also it requires feedback channel information which may cause extra delay.

$P(e|A_i)$ is the error probability given that A_i is the correct for the received symbol. Obviously, all symbols have an equal opportunity to send, so $P(A_i) = (1/4)$. For $P(e|A_i)$, we have

$$P(e|A_i) = \sum_{j \neq i} P\big(A_j|A_i\big) \tag{5}$$

where $P(A_i|A_j)$ refers to the probability that the received symbol should be in region A_j but be wrongly located in region A_i $(i, j = 1, 2, 3, 4$ and $i \neq j)$. For simplicity, we notate the symmetrical region for region A_i as region $A_{\bar{i}}$. Thanks to this symmetry, we have $P(A_i|A_j) = P(A_{\bar{i}}|A_{\bar{j}})$, where $i \neq j$ [e.g., $P(A_1|A_3) = P(A_4|A_2)$]. Placing (5) into (4) and applying the above property, the decoding error probability can be simplified as

$$P = \frac{1}{2}(P(e|A_3) + P(e|A_4)). \tag{6}$$

Here, $P(e|A_3)$ is the summation of $P(A_1|A_3)$, $P(A_2|A_3)$, and $P(A_4|A_3)$. In (6), $P(A_1|A_3)$, $P(A_4|A_3)$, and $P(e|A_4)$ can be directly calculated by the past work [47], [50]. So, we only need to calculate $P(A_2|A_3)$, i.e., the probability when the received symbol corresponding to the constellation point in A_3 (10) is located in A_2 (01) by mistake. Indeed, 10 and 01 are the most challenging cases to be distinguished for decoding.

To calculate $P(A_2|A_3)$, recall that the decoding error probability can be calculated by Craig's analytical model under the unit shape (Section III). However, the boundaries of decision regions in Craig's polar coordinate vary with the channel coefficients. Furthermore, the wedge shape of all decision regions [see Fig. 2(a)] is more complicated than a unit shape, making it difficult to calculate the decoding error probability.

To solve this problem, we start from the condition when $|H_1| \geq |H_2|$ and $0 \leq \phi \leq (\pi/2)$ (ϕ is the phase shift between H_1 and H_2).[5] Then, we extend our expression to other conditions, such as $|H_1| < |H_2|$ or $(\pi/2) < \phi \leq \pi$. Under each condition, we divide this condition into three cases for further simplification. For each case, we carefully partition the wedge decision regions into several unit shapes, and then we can apply Craig's analytical model to each divided unit shape, respectively. We detail the derivation for all conditions and cases in the Appendices.

The derivation reveals that $P(A_2|A_3)$ is a function of ϕ, $|H_1|$, and $|H_2|$. $P(A_1|A_3)$, $P(A_4|A_3)$, and $P(e|A_3)$ are similar. Therefore, the decoding error probability P is a function of ϕ, $|H_1|$, and $|H_2|$ based on (6). Due to the page limit, we do not show the detailed expression in the paper. For simplicity, we notate the expression of decoding error probability P as $P_f(\phi, |H_1|, |H_2|)$. Finally, the expression of P under all conditions can be calculated as

$$P = \begin{cases} P_f(\phi, |H_1|, |H_2|), & \text{if } |H_1| \geq |H_2|, 0 \leq |\phi| \leq \pi/2 \\ P_f(\pi - \phi, |H_1|, |H_2|), & \text{if } |H_1| \geq |H_2|, \pi/2 < |\phi| \leq \pi \\ P_f(\phi, |H_2|, |H_1|), & \text{if } |H_1| < |H_2|, 0 \leq |\phi| \leq \pi/2 \\ P_f(\pi - \phi, |H_2|, |H_1|), & \text{if } |H_1| < |H_2|, \pi/2 < |\phi| \leq \pi. \end{cases} \tag{7}$$

[5]For $\phi = 0$, all the possible constellation points are located on one line in the constellation map. So, we can directly employ the BER result from the existing solution [50].

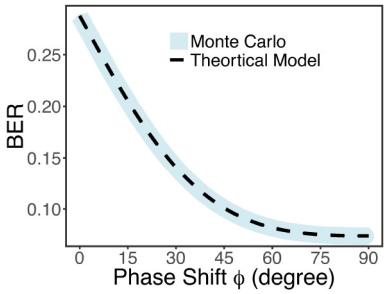

Fig. 4. Comparison result of the BER expression.

Here, the underlying intuition is that when using Craig's analytical model to derive the BER expression, we can leverage the symmetric property [31], [47] to easily extend the special case, e.g., $|H_1| \geq |H_2|$ and $0 \leq |\phi| \leq \pi/2$, to a general case by replacing the input parameters of the equation. By doing this, the derivation can be simplified significantly. This closed-form BER expression can be extended to higher modulations and multiple concurrent transmitters.

2) Validation of the BER Expression: To validate the proposed closed-form BER expression, we conduct Monte Carlo simulation and compare the simulation results with the BER expression. For simplicity, two transmitters have the same power and transmit signals under equal-gain channels (i.e., $|H_1| = |H_2|$) but varying phase shift, ϕ. We set the SNR of transmitted signals as 5 dB. The comparison results are shown in Fig. 4. The results from analysis and Monte Carlo simulation are very close to each other, which validates the correctness of the BER derivation. Note that in the Monte Carlo simulation, we also test other settings, such as different SNRs and power ratios of two transmitters, and all the simulation results are consistent with our BER expression.

3) Effect of the Phase Shift: Equation (7) reveals that the decoding error probability is determined by three factors: $|H_1|$, $|H_2|$, and ϕ. As mentioned earlier, controlling $|H_1|$ and $|H_2|$ requires strict closed-loop power control which may be impractical for the IoT devices. Therefore, we investigate the effect of phase shift ϕ on the decoding performance, given $|H_1|$ and $|H_2|$.

As shown in Fig. 5, we plot the BER curves under different SNRs according to (7). Here, $\text{SNR}_i = 10\log_{10}|H_i|^2/(2\sigma^2)$, $i = 1, 2$. In the following, we use SNR_i which is widely used in the communication systems instead of $|H_i|$. Our goal is to analyze the relationship between phase shift ϕ and the BER given SNR. Specifically, the SNR value varies from 5 to 25 dB. For the two transmitters, we randomly choose the SNR values within this range. Given each setting of SNR_1 and SNR_2, we vary the phase shift ϕ from 0° to 360° and plot the BER curve. We observe the following properties.

1) The BER during the process of increasing the phase shift is nonmonotonous. Two valleys appear when the phase shift $\phi = 90°$ and $\phi = 270°$. We call the range of ϕ corresponding to a lower BER as "good regions." Thus, the best choice of ϕ for the good regions is centered around 90° or 270°.

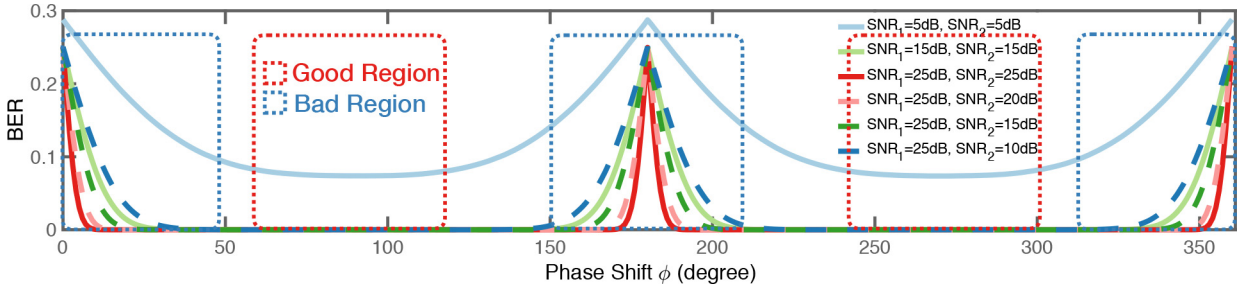

Fig. 5. Phase shift versus BER.

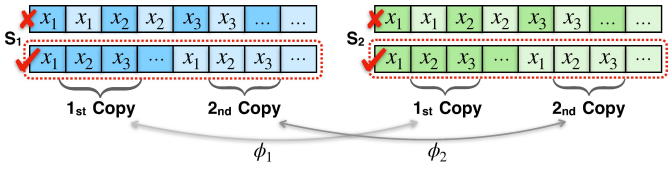

Fig. 6. Format of the two copies.

2) In contrast to good regions, the peaks occur at certain phase shift values, i.e., $\phi = 0°, 180°$. We call these phase shift ranges as "bad regions." The good regions and bad regions appear alternatively, and they are symmetrical with $\phi = 180°$.
3) For different SNR settings, the BER curves and the positions of good regions and bad regions follow the same trend, which indicates that the positions of good regions and bad regions are not affected by the SNR values. This suggests that we can manipulate the phase shift to achieve a high decoding performance even without knowing the channel conditions (i.e., SNRs).

To obtain a lower BER, the phase shift ϕ should lie in good regions, i.e., around 90° or 270°, for any given channel conditions.

B. Rotation-Code-Based Diversity Transmission

In practice, we cannot precisely manipulate the phase shift for maintaining the best values at the receiver. In fact, the phase shift is a random variable for each transmission and it follows a uniform distribution [33], [51]. To solve this, we propose a rotation-code-based diversity transmission, and then we leverage the diversity to guarantee the phase shift to be located in the good region.

1) Increasing the Diversity Gain: Recall that the good regions and bad regions are alternative and symmetrical. By utilizing this property, we let SigMix transmit two copies of the signal to increase the diversity gain. For simplicity, we denote the phase shift between the first copies of the transmitted signals as ϕ_1, and that between the second copies as ϕ_2. By doing so, we have a higher chance to guarantee that at least one phase shift (i.e., ϕ_1 or ϕ_2) is within the good regions.

Specifically, as shown in Fig. 6, to avoid the deep fading in the time domain, we directly insert a copy of the signal right after the original one instead of interleaving them. Here, the original signal refers to the first copy. For a given transmitter, the two consecutive copies from the same hardware and experience almost identical channel conditions, so the two consecutive superimposed signals will have almost identical phase shift. To increase the diversity gain, we need to guarantee that $\phi_1 \neq \phi_2$. To do so, we rotate the second copy of one transmitted signal with a certain angle and keep the other copies unchanged. Fig. 7 illustrates the idea of the rotation code. For the first copies from S_1 and S_2, the phase shift is ϕ_1. When we rotate the second copy from S_2 with angle β, the phase shift between the second copies from S_1 and S_2 is ϕ_2, which is equal to $\phi_1 + \beta$.

S_1 and S_2 can transmit either identical or different signals.

Fig. 7. Illustration of the rotation code.

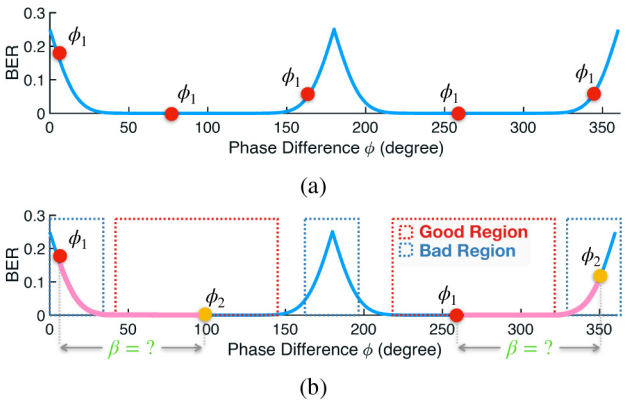

Fig. 8. Searching scheme for rotating angle β. (a) Possible phase differences for one copy. (b) Possible phase differences for two copies.

2) Optimal β: Up to now, we have two phase shifts ϕ_1 and ϕ_2. As shown in Fig. 8(b), the rotation code changes the phase shift between the second copies by β. However, we have no idea of the phase shift between the first copies ϕ_1 since it follows the uniform distribution. That is to say, ϕ_1 can be located at any position of the BER curve [see Fig. 8(a)]. Therefore, without known ϕ_1, we propose a searching scheme to find the optimal rotating angle β, so that we can guarantee that at least ϕ_1 or ϕ_2 is within the good regions. Specifically,

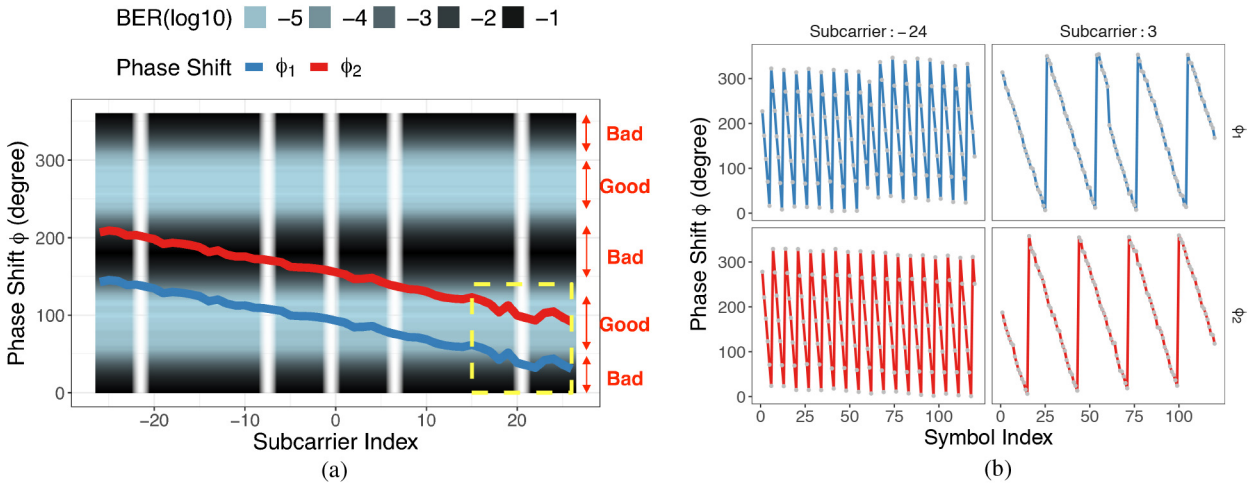

Fig. 9. Subcarriers' difference. (a) Phase shifts in different subcarriers. (b) Phase shifts vary with time.

we formulate this problem as an optimization problem

$$\begin{aligned} \min_{\beta} \quad & \{P(\phi_1), P(\phi_1+\beta)\} \\ \text{s.t.} \quad & 0^\circ \le \phi_1 < 360^\circ \\ & 0^\circ < \beta < 360^\circ \end{aligned} \tag{8}$$

where $P(.)$ is the BER given certain value of ϕ_1. Note that the size of the solution set is very small, only including hundreds of possible solutions, so a simple exhaustive search can solve this problem without causing any obvious computation overhead. By solving this, we can obtain an optimal value of θ that achieves the best average BER for any channel conditions.

The searching algorithm finds the optimal values 90° and 270° of β. Without loss of generality, we set $\beta = 90^\circ$ in our implementation. Note that the rotating angle β is different from the phase shift ϕ as shown in Fig. 3. The phase shift ϕ refers to the phase difference between two concurrent transmitted signals, while the rotating angle β is the phase difference between the first copy and second copy of one transmitted signal, and the other transmitters send two copies without rotation.

C. Adaptive Decoding

When the receiver receives the superimposed signal, there are two copies for each symbol. Which one should be used to decode the superimposed signal? Intuitively, the receiver can first calculate the phase shifts ϕ_1 and ϕ_2 based on the preambles, since the preambles of the transmitted signals can be made orthogonal to each other, making it easy to obtain the phase shifts separately. Then, the receiver decides which phase shift is in the good regions and selects the corresponding signal copy for decoding.

However, for OFDM systems, the channel behaviors of different subcarriers are different due to dynamic channel conditions and the frequency selective fading [11], [12]. Furthermore, the hardware imperfections exacerbate the differences among subcarriers. To see this clearly, we conduct a benchmark experiment and the detailed setup is introduced in Section VI-A. Fig. 9(a) plots the phase shifts (ϕ_1 and ϕ_2) in different subcarriers. For some subcarriers, ϕ_1 is in good regions, while for other subcarriers, ϕ_2 is in good regions. Furthermore, we randomly select two subcarriers (i.e., subcarrier −24 and subcarrier 3) and plot ϕ_1 and ϕ_2 for these two specific subcarriers under different time index (represented by the symbol index) as shown in Fig. 9(b). We observe that even for the same subcarrier, both ϕ_1 and ϕ_2 are not stable and vary with time. These experimental results reveal that the phase shifts not only vary with subcarriers but also with time. Therefore, using a fixed metric for all subcarriers at any given time, like prior work [31], [28] will result in a poor decoding performance. In contrast, in our design, the receiver decides which phase shift is in the good region for every subcarrier at any given time, and eventually selects the corresponding signal copies for decoding signals across different subcarriers. We summarize the adaptive signal copy selection in Algorithm 1. SigMix requires a traversal procedure of the packets to complete the adaptive signal copy selection. Fortunately, the procedure can be piggybacked to the signal decoding component, and the overhead of this traversal procedure is linearly increased and limited by the packet length.

Algorithm 1 Adaptive Signal Copy Selection

Input:
The sets of ϕ_1 and ϕ_2 for all subcarriers and all symbols in one packet, respectively, i.e., $\Phi_1 = \{\phi^k_{1[i]}\}$, $\Phi_2 = \{\phi^k_{2[i]}\}$; The good region of the phase shift R_{good};

Output:
The set of selected ϕ for all subcarriers and all symbols in one packet, $\Phi_{select} = \{\phi^k_{select[i]}\}$;

```
for i = 1 to packet_length do
    for k = 1 to number_of_subcarrier do
        if φ^k_{1[i]} ∈ R_good then
            φ^k_{select[i]} = φ^k_{1[i]};
        else
            φ^k_{select[i]} = φ^k_{2[i]};
        end if
    end for
end for
return Φ_select
```

Note that the two signal copies in SigMix share the same probability to be selected by the receiver, as the initial phase shift plays a critical role in making the signal copy located in a good region or a bad region, and the initial phase shift is random in low-cost IoT devices [33], [51].

V. Practical Issues

Decoding the superimposed signals demands a high synchronization accuracy, i.e., time synchronization, frequency synchronization, and phase synchronization [8]. However, in practice, the hardware imperfections of IoT devices will cause more challenges to achieve the required synchronization level.

Time Synchronization: To decode a superimposed signal, symbol-level time synchronization is needed [8], [9], [21]. For example, in Wi-Fi systems, time synchronization accuracy should be no larger than 2 ms. Recent work can achieve symbol-level synchronization for IoT devices. For example, a 300-ns accuracy for outdoor can be achieved by GPS clocks [52] and a below 200-ns accuracy for indoor can be achieved by Wi-Fi routers [53], [54]. In this article, for simplicity, we use a commercial clock which has a comparable performance with the mentioned solutions to achieve the required time synchronization. We provide more details in Section VI.

Frequency Synchronization and Phase Synchronization: Typically, losing frequency or phase synchronization mainly means that the signal has offsets [55], [56]. In particular, using a single-source signal as an example, three offsets exist when the oscillators of the transmitter and receiver keep drifting away from their clock at different speeds. Specifically, the CFO appears when downconverting signal from the carrier to the baseband, and the SFO happens when convert the analog signal into the digital one. Also, due to the limited processing ability of the hardware, the STO occurs when the receiver wrongly identifies the starting point of the signal. Note that CFO means losing the frequency synchronization, while SFO and STO mean losing the phase synchronization. Compensating these offsets has been well studied for the single source signal [57]. However, for superimposed signals, the traditional solutions cannot be applied any more. This is because applying a single compensation to different signal sources simultaneously will lead to a high decoding error rate.

To solve the above problem, intuitively, we can capture the offsets first and compensate the offsets with an average value to all the signal sources [9], [21]. However, the underlying assumption is that the transmitters should share exactly the same offsets, which maybe impractical for heterogeneous IoT devices. This is because each transmitter carries offsets with obvious different values. In contrast to the average compensation scheme, a promising solution is to dynamically decode the superimposed signal with the offsets [10]. In detail, instead of compensating the offsets on the superimposed signal, all the offsets can be reflected in the channel coefficients. By doing so, the receiver can directly decode the signal from different transmitters. Accordingly, SigMix addresses the offsets problem by leveraging the dynamic decoding to satisfy the requirements of the frequency and phase synchronization.

The above-mentioned scheme needs time-domain orthogonal preambles to accurately capture the offsets in the first place. Although this orthogonality would bring extra overhead, the overall preambles only cause less than 2% extra overhead of a single transmission given a standard Wi-Fi packet [46], which is accessible considering the improved throughput shown in Section VI. Moreover, the orthogonal preambles in the time domain [46] or the code domain [7] have been widely used in the concurrent transmission schemes to accurately capture the offsets and channel variations.

Fig. 10. Hardware in SigMix.

VI. Evaluation

A. Implementation

Hardware-Wise: We implement SigMix on a software-defined radio platform which consists of three universal software radio peripheral (USRPs) embedded with XCVR2450 daughter boards. Specifically, two USRP N210s connect to a laptop through a Gigabit Ethernet router as two transmitters, while one USRP N200 connects to another laptop through Ethernet cable as the receiver. For the time synchronization, each USRP that acts as a transmitter is connected to a central clock (i.e., NI CDA-2990) via SMA cables. We employ an HG2458RD-SM omnidirectional antenna with 3-dBi gain for each USRP. To be easily extended to other standard protocols, SigMix follows IEEE 802.11p standard, i.e., the 5.9-GHz carrier frequency and 10-MHz bandwidth. We control the SNR of the received signal around 10–20 dB, which is a common range in practice [58]. The hardware setup of SigMix is shown in Fig. 10.

Software-Wise: SigMix is built upon a recent Wi-Fi project programmed in GNU-radio [59]. Specifically, for SigMix transmitters, we implement the proposed rotation code as presented in Section IV-B. Each transmitter transmits two copies of the signal with a total length of 1500 bytes payload and a preamble, which follows the standard length of Wi-Fi packets. For SigMix receiver, we implement the adaptive decoding scheme as described in Section IV-C and compensate CFO, STO, and SFO as introduced in Section V. To focus on our design, we remove other schemes along with the Wi-Fi protocol for simplicity, such as scrambling, interleaving, channel coding, etc. The program is running on laptops operating on Ubuntu 16.04, and each laptop processes the data streams coming from the USRP. Note that processing the data stream by other low-cost boards, e.g., Raspberry Pi, is also feasible, as the GNU-radio is compatible to these platforms [60], [61].

Metrics: We use the following four metrics for the evaluation: 1) *BER:* The percentage of bits in error; here, the BER

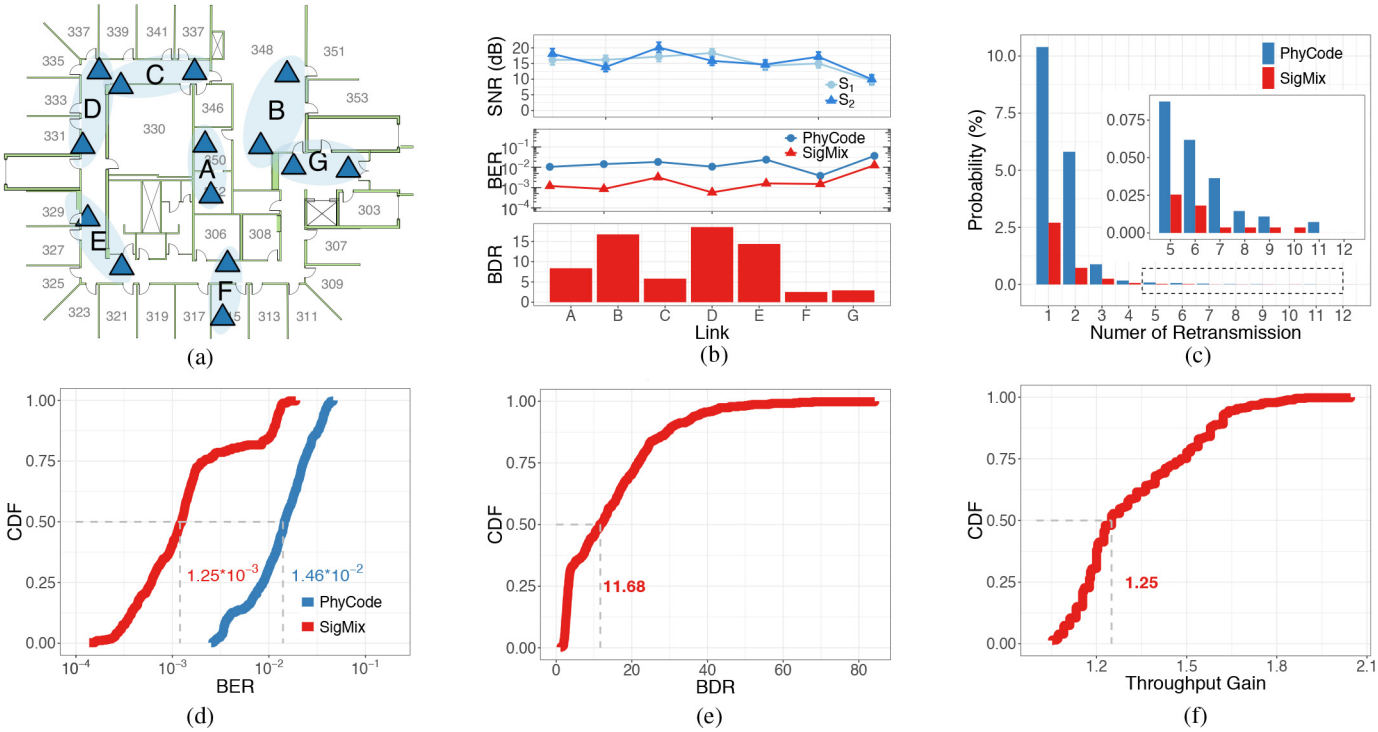

Fig. 11. Overall performance. (a) Deployment layout. (b) BER analysis for different links. (c) Number of retransmissions. (d) BER comparison. (e) BDR. (f) Throughput gain.

refers to the raw BER without considering the channel coding; 2) *BER Decline Ratio (BDR):* Defined as the ratio of BER in the existing scheme to BER in SigMix; 3) *Throughput Gain:* The ratio of throughput in SigMix to throughput in the existing scheme, while keeping the traffic pattern constant; and 4) *Delay Distribution:* The number of retransmissions until the packet is successfully received. Note that both BER and BDR are related to the reliability, while throughput gain and delay distribution refer to the efficiency and delay of the system performance, respectively.

We evaluate SigMix in comparison with the state-of-the-art PNC and NOMA schemes.

1) *Traditional PNC (T-PNC):* We denote the traditional PNC scheme as T-PNC, which utilizes the benefit of superimposed signals for bidirectional relay networks [9], [21]. To be fair, we enable T-PNC to decode the superimposed signal at the relay node directly and leave the offset compensation unchanged. T-PNC only compensates an average CFO, while it does not consider other offsets or the rotation code. Consequently, it may not perform well in practical scenarios.
2) *PhyCode:* PhyCode [10] is a new type of NOMA without power control, where the superimposed signal can be decoded directly at the receiver. In contrast to T-PNC, PhyCode addresses CFO, SFO, and STO as well. But it assumes that the constellation points are distinguishable. So, it decodes the superimposed signal without considering the rotation code to increase the diversity gain. Note that the relay node in T-PNC and the receiver in PhyCode is the same node which receives superimposed signals from concurrent transmitters.

Methodology: Our goal is to evaluate the performance of SigMix for decoding the superimposed signal across different scenarios. First, we evaluate SigMix in indoor dynamic environments with rich multipath effects. Specifically, we conduct the experiments in an office building and we randomly select seven regions, including both line-of-sight and non-line-of-sight scenarios, as shown in Fig. 11(a). For each region, we deploy two transmitters and one receiver. The distance between the transmitters and receiver varies from 1 to 10 m. To guarantee independent channels, we keep the distance between two transmitters no less than 20 cm which is much larger than the signal wavelength (i.e., 5.1 cm for the 5.9-GHz wireless signal). For deployment simplicity, i.e., a shorter cable length, we set the distance between two transmitters as 20 and 30 cm in the following experiments. Note that we also conducted experiments with larger distances, say 3 m, and there is no obvious difference. This is because the larger distance only results in a longer propagation delay, around tens of nanoseconds, and it can be addressed by SigMix as detailed in Section V. To mimic IoT traffic with periodic data, the transmitter transmits one packet per second. For each region, the experiment lasts for one hour (i.e., 3600 rounds of concurrent transmissions) and the total experiment lasts for 7 h. During the experiments, people in the building either sit in their desk space or walk around the corridors as usual, which contributes to a dynamic indoor environment [62], [63]. Second, to focus on the influence of SNR and avoid the environmental noise, we deploy SigMix in an anechoic chamber. The SNR is adjusted by changing

TABLE II
COMPARISON OF BER

	Scheme		
Metric	T-PNC	PhyCode	**SigMix**
BER	3.82×10^{-1}	1.43×10^{-2}	1.05×10^{-3}

the transmission power. For each SNR setting, the experiment lasts for one hour. Finally, we evaluate SigMix under outdoor mobile scenarios. Specifically, we deploy the transmitters and the receiver in two vehicles. The two vehicles are driven along a ring road in a city.

B. Overall Performance

We compare the decoding performance of T-PNC, PhyCode, and the proposed SigMix under the indoor deployment.

BER and BDR: As shown in Table II, we summarize the average BER from all seven regions for each scheme. Obviously, the BER of T-PNC is much higher since it does not address CFO, SFO, and STO very well, especially in the presence of low-cost IoT devices that have high and heterogeneous offsets. Compared with T-PNC, PhyCode achieves a lower BER as it solves the offset problem. The BER of SigMix is significantly lower when compared with T-PNC and PhyCode, since it not only addresses the offsets well but also leverages the rotation code and the diversity gain to further reduce the BER. In the following comparisons, we only show the results of PhyCode and SigMix because both solutions deal with the offset problem elegantly.

Fig. 11(d) plots the CDF of BER from all seven regions. As we can see, SigMix has a median BER of 1.25×10^{-3}, outperforming PhyCode by $11.68\times$. In other words, SigMix achieves a one-order lower BER. This is because SigMix utilizes the rotation code and adaptive decoding scheme, making it more robust against dynamic channel conditions and hardware imperfections. To see the improvement clearly, Fig. 11(e) shows the CDF of the BDR. Furthermore, Fig. 11(b) illustrates the BER analysis of each deployed region. As we can see, the SNRs of the two signals, S_1 and S_2, vary in different deployed regions due to the different environmental noises and layouts. In all the seven deployed regions, the BER of SigMix outperforms PhyCode and the corresponding BDR is 9.91 on average. It is worth noting that in region *G*, the BER of SigMix slightly increases and close to that of PhyCode. This is because there are more environmental noises in region *G*, making the cluster of a constellation point more sparse.

Throughput Gain: We perform the trace-driven simulations to investigate the throughput gain of SigMix. Specifically, we record the bit error information of 25 000 packets from USRP testbed for each scheme. For each transmitter, we emulate 25 000 packets applying the CRC-32 algorithm and convolutional codes with 1/2 code rates (common settings in Wi-Fi) in MATLAB. Then, we use the recorded bit error information as the physical-layer decoding results. By using the Viterbi decoding and checking the CRC, we can obtain the packet loss results. The throughput gain is calculated according to the packet loss results of SigMix and PhyCode. As shown in Fig. 11(f), the median throughput gain of SigMix is 1.25, which indicates a high efficiency of the system.

Number of Retransmissions: Similar to the throughput gain, we perform the trace-driven simulations to compare the delay distribution of SigMix and PhyCode. We calculate the number of retransmissions of both schemes based on their packet loss results. Fig. 11(c) shows the number of retransmissions for each lost packet till a success. As we can see, for all numbers of retransmissions, the probability of SigMix is lower than that of PhyCode, implying a lower delay of the transmission. Specifically, the probability of retransmitting once and twice of SigMix is $3.84\times$ and $7.98\times$ lower than that of PhyCode, respectively. Note that the BER determines both the throughput gain and the number of retransmissions and, thus, we only show the BER analysis in the following comparisons.

C. Impact of the Signal SNR and the SNR ratio

Unlike traditional NOMA techniques (i.e., SIC) which require a substantially different received power levels of the two signals [6], [14], SigMix can perform well without power control of the transmitters. To demonstrate that we evaluate the influence both of the SNR and the SNR ratio of two transmitted signals on the decoding performance. To avoid environmental interference, we conduct the experiments in the anechoic chamber shown in Fig. 12(a). First, for the evaluation of the SNR influence, we manually tune the SNR of the two transmitters from 5 to 15 dB. As shown in Fig. 12(b), SigMix outperforms PhyCode under different SNRs. The BER of both SigMix and PhyCode is reduced as the SNR increases. One thing worth noting is that when the SNR is lower, the BDR becomes smaller as well. The reason is that when the SNR is under a lower level, the environmental noise plays a vital role in distorting the signal, making the cluster of a constellation point more sparse. Overall, with the typical SNR range [22] (e.g., above 5 dB), the BDR of our scheme is high. Second, for the evaluation of the SNR ratio influence, we keep the SNR of one transmitter stable and change the other one gradually. The SNR difference between two transmitters is within 5 dB to avoid a big signal strength gap. We show the comparison results in Fig. 12(c). SigMix outperforms PhyCode in any given SNR ratio. More importantly, the BER is not changed obviously by the SNR ratio, which reveals that SigMix is robust to the SNR ratio.

D. Impact of the Packet Length

To evaluate the effect of packet length on the decoding performance, we keep the SNR of two transmitters stable and vary the packet length from 10 to 1500 bytes. This experiment was conducted in an ordinary office. From Fig. 13, we observe that SigMix always outperforms PhyCode for any given packet length. The BER of SigMix becomes much smaller when we reduce the packet length (e.g., the BER is 10^{-5} with a packet length of 10 bytes). This is because, with the growth of the packet length, the damage of residual offsets becomes more obvious. But even with the longest packet length in our experiment (i.e., following the Wi-Fi standard), SigMix can still achieve a better BDR, and a considerable low BER result, which verifies that SigMix compensates CFO, SFO, and STO very well.

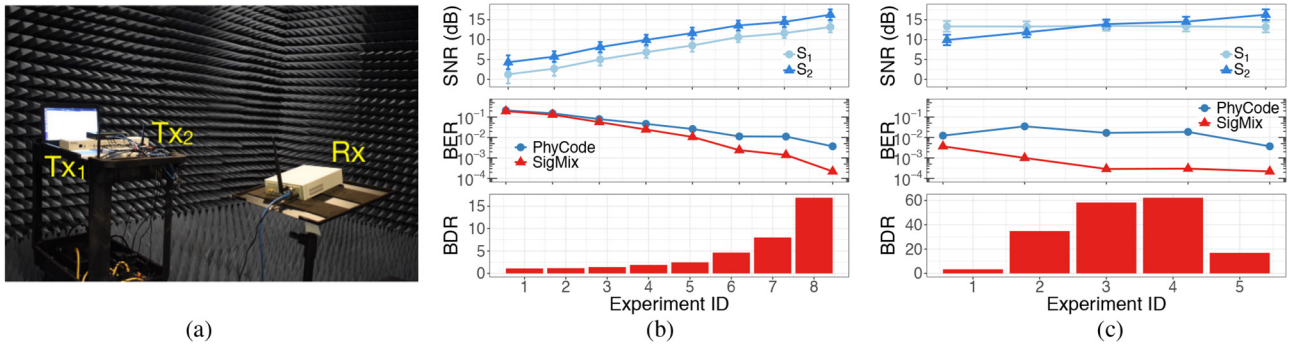

Fig. 12. Performance under different SNRs and SNR ratios. (a) Setup in the chamber. (b) Impact of SNR. (c) Impact of SNR ratio.

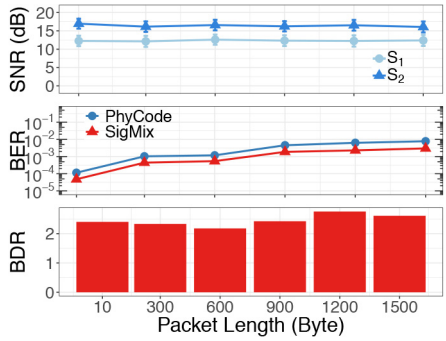

Fig. 13. Performance of different packet lengths.

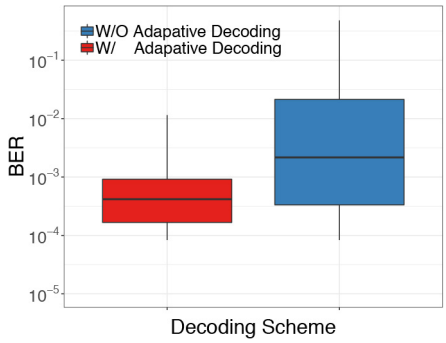

Fig. 14. W/ and W/O adaptive decoding scheme.

E. Impact of the Subcarriers' Difference

To validate the effectiveness of the proposed adaptive decoding scheme, we conducted the experiment in an ordinary office with rich multipath. As we can see from Fig. 14, the average BER is higher and its variation is larger when without applying the adaptive decoding scheme, even if we compensate the offsets well and apply the rotation code. In contrast, after applying the adaptive decoding scheme, the BER of SigMix becomes lower, which demonstrates that SigMix can precisely respond to the subcarriers' difference to achieve high decoding performance.

F. Outdoor Mobile Scenario

To evaluate the mobility on the decoding performance, we deploy the transmitters and receiver in two vehicles and the setup is shown in Fig. 15(a). During the road experiment, the two vehicles are continuously driven along a ring road for ten rounds [see Fig. 15(b)] with a maximum speed at 40 km/h. As shown in Fig. 15(c), the SNRs of the two transmitters vary from -10 to 20 dB due to the mobility effect. The median SNRs of the two transmitters are 15.52 and 13.23 dB, respectively. Fig. 16 illustrates the comparison of the BER. SigMix has a median BER of 4.51×10^{-3} and a median BDR of 2.48, outperforming PhyCode. Overall, SigMix can perform well in the presence of mobility.

VII. Discussion and Future Work

This article introduces a practical solution for decoding the superimposed signal in the presence of dynamic channel conditions and hardware imperfections in the IoT systems. We list some of our insights below for the discussion and future research work.

Overhead: In SigMix, we transmit two copies of each signal to achieve a high decoding performance, which appears to be less efficient. However, the two-copy diversity transmissions are desirable for the following reasons. First, many IoT transmission schemes start the transmission by blindly sending the same packet multiple times to achieve a desirable BER [64]–[67]. Compared to them, transmitting two copies within one transmission reduces the delay and does not occupy more bandwidth. Second, compared with the past work that relied on retransmission to decode superimposed signals [9], [34], SigMix consumes much less transmission power and has a low overall communication latency, crucial to many time-sensitive or real-time applications.

Modulation Schemes: In this article, we focus more on the low-order modulation, i.e., two BPSK modulated concurrent signals. The advanced modulation scheme for superimposed signals [29], [35], e.g., 16-QAM or 64-QAM, can offer a higher throughput gain, but it also requires a strict signal strength control. However, the dynamic channel conditions and hardware imperfections make the signal strength control much challenging in IoT scenarios. Therefore, how to balance the modulation scheme and the varying signal strength needs to be investigated in future studies. Moreover, compared to many low-data rate technologies in IoT, e.g., RFID, LoRa, ZigBee, etc., SigMix can offer a much higher data rate by leveraging the wideband technology, i.e., OFDM. To this end, by using the low-order modulation alone, the data rate of SigMix is sufficient to be applied to many IoT applications.

Fig. 15. Outdoor Setup. (a) Setup for vehicles. (b) Road experiments. (c) SNR.

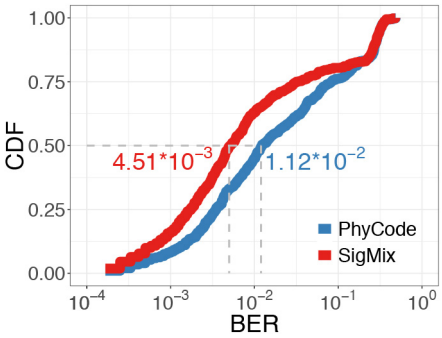

Fig. 16. Performance in vehicles.

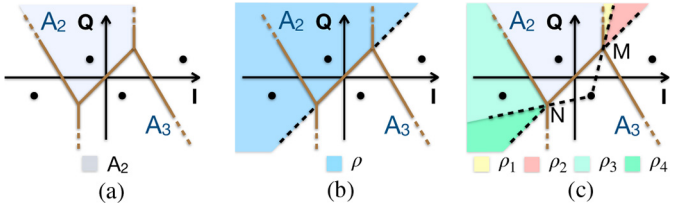

Fig. 17. Two-step partition method for case 1. (a) Origin. (b) Step 1. (c) Step 2.

Soft-Value Decoding: In SigMix, we select one copy whose phase shift is in the good regions to decode the superimposed signal. To further utilize the diversity gain of our scheme, we can apply many soft-value combining schemes to further reduce the BER [68], [69] under strong environmental noise. Specifically, two copies can be utilized together based on their soft values to decode the superimpose signal. We leave this part of work as one of our future works.

MAC-Layer Design and Other Coding Schemes: So far, the implementation of SigMix is focused on the physical layer. To further boost the performance and expand the applications of our system, more research on how to apply sophisticated channel coding and MAC-layer protocols to our system is needed. With the newly proposed testbed [70], we can further implement MAC-layer protocols and we leave this for further work.

Scale to a Large Network: We implement SigMix in a two-transmitter system. By leveraging a fine-designed orthogonal preamble, e.g., code-domain orthogonal [7], and distributed time clocks, e.g., GPS clocks, we can involve more transmitters to transmit signal concurrently and decode the superimposed signal. Moreover, involving more antennas with more RF chains can also enable us to utilize the spatial spectrum resource. This will be an important future research issue.

VIII. Conclusion

This article presented SigMix, a practical solution to decode the superimposed signal in the presence of dynamic channel conditions and hardware imperfections in IoT systems. We demonstrated the effectiveness of our design through the implementation on a software-defined radio platform. SigMix is promising toward addressing the grand challenge of IoT applications, such as the spectrum efficiency, delay, and reliability, achieving an 11.68× improvement in the median BER compared to the state-of-the-art.

Appendix A
BER Expression in Case 1

Under the condition that $|H_1| \geq |H_2|$ and $0 \leq \phi \leq (\pi/2)$, we can further divide this condition into three cases based on the phase shift ϕ as follows [47]:

$$\begin{cases} \text{Case 1:} & \cos\phi > \frac{|H_1|}{2|H_2|} \\ \text{Case 2:} & \frac{|H_2|}{2|H_1|} \leq \cos\phi \leq \frac{|H_1|}{2|H_2|} \\ \text{Case 3:} & \cos\phi < \frac{|H_2|}{2|H_1|}. \end{cases} \tag{9}$$

Given each case, the boundaries of decision regions are now fixed in Craig's polar coordinate. So, we can calculate $P(A_2|A_3)$ for the three cases, separately.

To divide the decision regions properly, let us start from case 1. As shown in Fig. 17, to calculate $P(A_2|A_3)$, we design a two-step partition method. In the first step, as shown in Fig. 17(b), we extend the boundary between regions A_2 and A_3. By doing so, we can obtain a new region in the constellation map, i.e., region ρ. In the second step, as shown in Fig. 17(c), we connect the location of 10 to the two intersections (i.e., point M and point N) and extend these two lines. Then, we obtain regions ρ_1, ρ_2, ρ_3, and ρ_4, respectively. Obviously, each region ρ_i is a unit shape. The region ρ contains five regions, including region A_2, regions ρ_1, ρ_2, ρ_3, and ρ_4. Therefore, we have

$$P(A_2|A_3) = P(\rho|A_3) - \sum_{i=1}^{4} P(\rho_i|A_3) \tag{10}$$

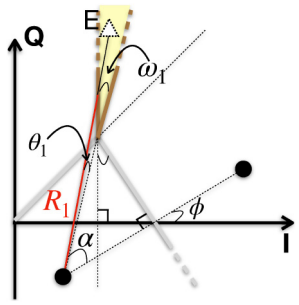

Fig. 18. Zoom in to region ρ_1.

where $P(\rho|A_3)$ can be calculated by [50]. Next, we can directly apply Craig's analytical model to calculate $P(\rho_i|A_3)$ since each region ρ_i is a unit shape. Here, taking $P(\rho_1|A_3)$ as an example (see Fig. 18), we have

$$P(\rho_1|A_3) = \frac{1}{2\pi}\int_0^{\omega_1} \exp\left(-\frac{{R_1}^2(\theta)}{2\sigma^2}\right)d\theta \tag{11}$$

where ${R_1}^2(\theta)$ and ω_1 can be calculated based on the analytic geometry [47], i.e., ${R_1}^2(\theta) = ([(|H_1|-2|H_2|\cos\phi)^2]/[\sin^2\theta])$ and $\omega_1 = \pi/2 - \alpha - \phi$. Here, $\alpha = \arctan[(|H_1| - |H_2|\cos\phi)/(|H_2|\sin\phi)]$.

Similar to the calculation of $P(\rho_1|A_3)$, we can calculate $P(\rho_i|A_3), i = 2, 3, 4$ in the same way. Specifically, we first derive the expressions of ${R_i}^2(\theta), i = 2, 3, 4$ based on simple analytic geometry, and then we can obtain the expression of $P(\rho_i|A_3)$ based on (3) as follows:

$$\begin{cases} P(\rho_2|A_3) = \frac{1}{2\pi}\int_0^{\omega_2} \exp\left[-\frac{|H_1|^2-2|H_1||H_2|\cos\phi+|H_2|^2}{2\sigma^2\sin^2\theta}\right]d\theta \\ P(\rho_3|A_3) = \frac{1}{2\pi}\int_0^{\omega_3} \exp\left[-\frac{(2|H_1|\cos\phi-|H_2|)^2}{2\sigma^2\sin^2\theta}\right]d\theta \\ P(\rho_4|A_3) = \frac{1}{2\pi}\int_0^{\omega_4} \exp\left[-\frac{|H_1|^2-2|H_1||H_2|\cos\phi+|H_2|^2}{2\sigma^2\sin^2\theta}\right]d\theta \end{cases} \tag{12}$$

where ω_i can be also calculated using the analytic geometry as follows:

$$\begin{cases} \omega_2 = \arcsin\left(\frac{\cos\alpha\sqrt{|H_1|^2-2|H_1||H_2|\cos\phi+|H_2|^2}}{|H_2|}\right) \\ \omega_3 = \alpha + 2\arccos\left(\frac{\cos\alpha\sqrt{|H_1|^2-2|H_1||H_2|\cos\phi+|H_2|^2}}{|H_2|}\right) - \frac{\pi}{2} \\ \omega_4 = \arcsin\left(\frac{\cos\alpha\sqrt{|H_1|^2-2|H_1||H_2|\cos\phi+|H_2|^2}}{|H_2|}\right). \end{cases} \tag{13}$$

So far we have calculated $P(A_2|A_3)$ for case 1. By placing (10) and (11) and combining the calculation results in [47] and [50], we can derive the detailed expression of P for case 1.

Similarly, for cases 2 and 3, we can also divide all the decision regions into several unit shapes and repeat the above derivation process to calculate $P(A_2|A_3)$. We show the partition process and expressions in the following section.

Appendix B
Region Partition for Case 2 and Case 3

For case 2, we also use the proposed two-step partition method to divide the decision regions into several unit shapes.

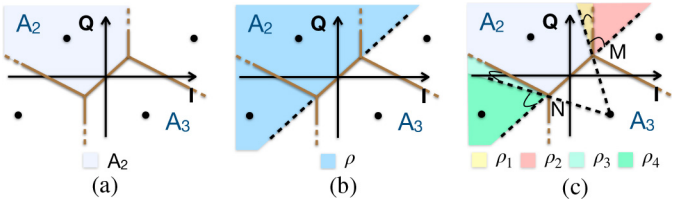

Fig. 19. Region partition for case 2. (a) Origin. (b) Step 1. (c) Step 2.

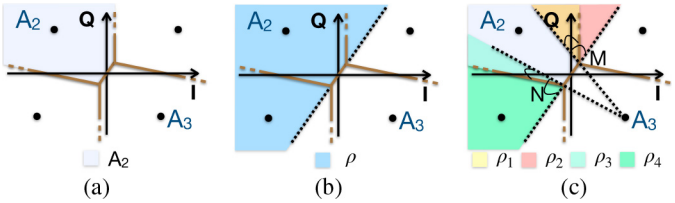

Fig. 20. Region partition for case 3. (a) Origin. (b) Step 1. (c) Step 2.

As shown in Fig. 19(b) and (c), region ρ contains four regions, including regions A_2, ρ_2, ρ_3, and ρ_4. We denote the overlapped region between A_2 and ρ_2 as ρ_1. So, we have

$$\begin{aligned} P(A_2|A_3) = {} & P(\rho|A_3) - P(\rho_2|A_3) - P(\rho_3|A_3) \\ & - P(\rho_4|A_3) + P(\rho_1|A_3). \end{aligned} \tag{14}$$

From Fig. 19(c), we note that only the shape of region ρ_1 has been changed compared with case 1 [see Fig. 17(c)]. Therefore, for case 2, we only need to update $P(\rho_1|A_3)$ as follows, while other items are the same with that of case 1

$$P(\rho_1|A_3) = \frac{1}{2\pi}\int_0^{\omega_1} \exp\left[-\frac{(|H_1| - 2|H_2|\cos\phi)^2}{2\sigma^2\sin^2\theta}\right]d\theta \tag{15}$$

where ω_1 is updated as $\omega_1 = \alpha + \phi - (\pi/2)$.

Similarly, for case 3, the region partition is shown in Fig. 20. Obviously, region ρ contains three regions, including regions A_2, ρ_2, and ρ_4. We denote the overlapped region between ρ_2 and A_2 as ρ_1, while the overlapped region between ρ_4 and A_2 as ρ_3. So, we have

$$\begin{aligned} P(A_2|A_3) = {} & P(\rho|A_3) - P(\rho_2|A_3) - P(\rho_4|A_3) \\ & + P(\rho_1|A_3) + P(\rho_3|A_3). \end{aligned} \tag{16}$$

From Fig. 20(c), we observe that only the shape of region ρ_3 has been changed compared with case 2 in Fig. 19(c). Therefore, in (16), $P(\rho|A_3)$, $P(\rho_2|A_3)$, and $P(\rho_4|A_3)$ are the same as that of both cases 1 and 2, while $P(\rho_1|A_3)$ is the same as that of case 2. So, for case 3, we only need to update $P(\rho_3|A_3)$ as

$$P(\rho_3|A_3) = \frac{1}{2\pi}\int_0^{\omega_3} \exp\left[-\frac{(|H_2| - 2|H_1|\cos\phi)^2}{2\sigma^2\sin^2\theta}\right]d\theta \tag{17}$$

where ω_3 can be updated as

$$\begin{aligned} \omega_3 = {} & \frac{\pi}{2} - \alpha - 2\arccos \\ & \times \left(\frac{\cos\alpha\sqrt{|H_1|^2 - 2|H_1||H_2|\cos\phi + |H_2|^2}}{|H_2|}\right). \end{aligned} \tag{18}$$

REFERENCES

[1] C. V. Forecast *et al.*, *Cisco Visual Networking Index: Global Mobile Data Traffic Forecast Update 2017–2022*, Cisco, San Jose, CA, USA, 2019.

[2] M. Torchia and M. Shirer, *IDC Forecasts Worldwide Technology Spending on the Internet of Things to Reach 1.2 Trillion in 2022*, IDC Media Center, Gurugram, Haryana, 2018.

[3] S. Ray, J. B. Carruthers, and D. Starobinski, "RTS/CTS-induced congestion in ad hoc wireless LANs," in *Proc. IEEE Wireless Commun. Netw. (WCNC)*, vol. 3, 2003, pp. 1516–1521.

[4] S. Gollakota and D. Katabi, "ZigZag decoding: Combating hidden terminals in wireless networks," in *Proc. SIGCOMM*, vol. 38, 2008, pp. 159–170.

[5] J. Jang and F. Adib, "Underwater backscatter networking," in *Proc. ACM Special Interest Group Data Commun.*, 2019, pp. 187–199.

[6] S. Sen, N. Santhapuri, R. R. Choudhury, and S. Nelakuditi, "Successive interference cancelation: A back-of-the-envelope perspective," in *Proc. 9th ACM SIGCOMM Workshop Hot Topics Netw.*, 2010, p. 17.

[7] T. Das *et al.*, "CoReCast: Collision resilient broadcasting in vehicular networks," in *Proc. 16th Annu. Int. Conf. Mobile Syst. Appl. Services*, 2018, pp. 217–229.

[8] S. Zhang, S. C. Liew, and P. P. Lam, "Hot topic: Physical-layer network coding," in *Proc. ACM 12th Annu. Int. Conf. Mobile Comput. Netw.*, 2006, pp. 358–365.

[9] L. You, S. C. Liew, and L. Lu, "Reliable physical-layer network coding supporting real applications," *IEEE Trans. Mobile Comput.*, vol. 16, no. 8, pp. 2334–2350, Aug. 2016.

[10] W. Cui, C. Liu, L. Cai, and J. Pan, "PhyCode: A practical wireless communication system exploiting superimposed signals," in *Proc. IEEE Int. Conf. Commun. (ICC)*, 2019, pp. 1–6.

[11] D. Halperin, W. Hu, A. Sheth, and D. Wetherall, "Predictable 802.11 packet delivery from wireless channel measurements," *ACM SIGCOMM Comput. Commun. Rev.*, vol. 41, no. 4, pp. 159–170, 2011.

[12] J. Wang *et al.*, "LiFS: Low human-effort, device-free localization with fine-grained subcarrier information," in *Proc. 22nd Annu. Int. Conf. Mobile Comput. Netw.*, 2016, pp. 243–256.

[13] W. Zhou, T. Das, L. Chen, K. Srinivasan, and P. Sinha, "BASIC: Backbone-assisted successive interference cancellation," in *Proc. 22nd Annu. Int. Conf. Mobile Comput. Netw.*, 2016, pp. 149–161.

[14] Y. Saito, Y. Kishiyama, A. Benjebbour, T. Nakamura, A. Li, and K. Higuchi, "Non-orthogonal multiple access (NOMA) for cellular future radio access," in *Proc. IEEE 77th Veh. Technol. Conf. (VTC Spring)*, 2013, pp. 1–5.

[15] M. Shafi *et al.*, "5G: A tutorial overview of standards, trials, challenges, deployment, and practice," *IEEE J. Sel. Areas Commun.*, vol. 35, no. 6, pp. 1201–1221, Jun. 2017.

[16] L. Dai, B. Wang, Y. Yuan, S. Han, I. Chih-Lin, and Z. Wang, "Non-orthogonal multiple access for 5G: Solutions, challenges, opportunities, and future research trends," *IEEE Commun. Mag.*, vol. 53, no. 9, pp. 74–81, Sep. 2015.

[17] L. P. Qian, Y. Wu, H. Zhou, and X. Shen, "Non-orthogonal multiple access vehicular small cell networks: Architecture and solution," *IEEE Netw.*, vol. 31, no. 4, pp. 15–21, Jul./Aug. 2017.

[18] Z. Ding *et al.*, "Application of non-orthogonal multiple access in LTE and 5G networks," *IEEE Commun. Mag.*, vol. 55, no. 2, pp. 185–191, Feb. 2017.

[19] P. Hu, P. Zhang, and D. Ganesan, "Laissez-faire: Fully asymmetric backscatter communication," *ACM SIGCOMM Comput. Commun. Rev.*, vol. 45, no. 4, pp. 255–267, 2015.

[20] Z. Song, L. Shangguan, and K. Jamieson, "Wi-Fi goes to town: Rapid picocell switching for wireless transit networks," in *Proc. Conf. ACM Special Interest Group Data Commun.*, 2017, pp. 322–334.

[21] L. Lu, T. Wang, S. C. Liew, and S. Zhang, "Implementation of physical-layer network coding," *Phys. Commun.*, vol. 6, pp. 74–87, Mar. 2013.

[22] S. Katti, S. Gollakota, and D. Katabi, "Embracing wireless interference: Analog network coding," *ACM SIGCOMM Comput. Commun. Rev.*, vol. 37, no. 4, pp. 397–408, 2007.

[23] L. Chen, F. Wu, J. Xu, K. Srinivasan, and N. Shroff, "BiPass: Enabling end-to-end full duplex," in *Proc. 23rd Annu. Int. Conf. Mobile Comput. Netw.*, 2017, pp. 114–126.

[24] M. Hessar, A. Najafi, and S. Gollakota, "NetScatter: Enabling large-scale backscatter networks," in *Proc. NSDI*, 2019, pp. 271–284.

[25] M. Jin, Y. He, X. Meng, D. Fang, and X. Chen, "Parallel backscatter in the wild: When burstiness and randomness play with you," in *Proc. ACM 24th Annu. Int. Conf. Mobile Comput. Netw.*, 2018, pp. 471–485.

[26] C. E. Shannon *et al.*, "Two-way communication channels," in *Proc. 4th Berkeley Symp. Math. Stat. Probab.*, vol. 1, 1961, pp. 611–644.

[27] E. C. Van Der Meulen, "Three-terminal communication channels," *Adv. Appl. Probab.*, vol. 3, no. 1, pp. 120–154, 1971.

[28] H. Zhang and L. Cai, "Design of channel coded heterogeneous modulation physical layer network coding," *IEEE Trans. Veh. Technol.*, vol. 67, no. 3, pp. 2219–2230, Mar. 2018.

[29] H. Zhang, L. Zheng, and L. Cai, "Design and analysis of hierarchical physical layer network coding," *IEEE Trans. Wireless Commun.*, vol. 16, no. 12, pp. 7966–7981, Dec. 2017.

[30] H. Zhang and L. Cai, "Bi-directional multi-hop wireless pipeline using physical-layer network coding," *IEEE Trans. Wireless Commun.*, vol. 16, no. 12, pp. 7950–7965, Dec. 2017.

[31] A. Y.-C. Peng, S. Yousefi, and I.-M. Kim, "On error analysis and distributed phase steering for wireless network coding over fading channels," *IEEE Trans. Wireless Commun.*, vol. 8, no. 11, pp. 5639–5649, Nov. 2009.

[32] D. Tse and P. Viswanath, *Fundamentals of Wireless Communication*. Cambridge, U.K.: Cambridge Univ. Press, 2005.

[33] T. H. Lee and A. Hajimiri, "Oscillator phase noise: A tutorial," *IEEE J. Solid-State Circuits*, vol. 35, no. 3, pp. 326–336, Mar. 2000.

[34] H. Pan, L. Lu, and S. C. Liew, "Practical power-balanced non-orthogonal multiple access," *IEEE J. Sel. Areas Commun.*, vol. 35, no. 10, pp. 2312–2327, Oct. 2017.

[35] H. Pan, L. Lu, and S. C. Liew, "Network-coded multiple access with high-order modulations," *IEEE Trans. Veh. Technol.*, vol. 66, no. 11, pp. 9776–9792, Nov. 2017.

[36] H. Pan, S. C. Liew, J. Liang, Y. Shao, and L. Lu, "Network-coded multiple access on unmanned aerial vehicle," *IEEE J. Sel. Areas Commun.*, vol. 36, no. 9, pp. 2071–2086, Sep. 2018.

[37] R. Eletreby, D. Zhang, S. Kumar, and O. Yağan, "Empowering low-power wide area networks in urban settings," in *Proc. Conf. ACM Special Interest Group Data Commun.*, 2017, pp. 309–321.

[38] J. Wang, H. Hassanieh, D. Katabi, and P. Indyk, "Efficient and reliable low-power backscatter networks," in *Proc. ACM SIGCOMM Conf. Appl. Technol. Archit. Protocols Comput. Commun.*, 2012, pp. 61–72.

[39] M. Jin, Y. He, X. Meng, Y. Zheng, D. Fang, and X. Chen, "FlipTracer: Practical parallel decoding for backscatter communication," *IEEE/ACM Trans. Netw.*, vol. 27, no. 1, pp. 330–343, Feb. 2019.

[40] L. Kong and X. Liu, "mZig: Enabling multi-packet reception in ZigBee," in *Proc. 21st Annu. Int. Conf. Mobile Comput. Netw.*, 2015, pp. 552–565.

[41] F. Adelantado, X. Vilajosana, P. Tuset-Peiro, B. Martinez, J. Melia-Segui, and T. Watteyne, "Understanding the limits of LoRaWAN," *IEEE Commun. Mag.*, vol. 55, no. 9, pp. 34–40, Sep. 2017.

[42] D. Vasisht *et al.*, "FarmBeats: An IoT platform for data-driven agriculture," in *Proc. 14th USENIX Symp. Netw. Syst. Design Implement. (NSDI)*, 2017, pp. 515–529.

[43] S. Gollakota, S. D. Perli, and D. Katabi, "Interference alignment and cancelation," *ACM SIGCOMM Comput. Commun. Rev.*, vol. 39, no. 4, pp. 159–170, 2009.

[44] H. Hassanieh, O. Abari, M. Rodriguez, M. Abdelghany, D. Katabi, and P. Indyk, "Fast millimeter wave beam alignment," in *Proc. Conf. ACM Special Interest Group Data Commun.*, 2018, pp. 432–445.

[45] E. Hamed, H. Rahul, and B. Partov, "Chorus: Truly distributed distributed-MIMO," in *Proc. Conf. ACM Special Interest Group Data Commun.*, 2018, pp. 461–475.

[46] H. Rahul, H. Hassanieh, and D. Katabi, "SourceSync: A distributed wireless architecture for exploiting sender diversity," *ACM SIGCOMM Comput. Commun. Rev.*, vol. 41, no. 4, pp. 171–182, 2011.

[47] M. Park, I. Choi, and I. Lee, "Exact BER analysis of physical layer network coding for two-way relay channels," in *Proc. IEEE 73rd Veh. Technol. Conf. (VTC Spring)*, 2011, pp. 1–5.

[48] J. W. Craig, "A new, simple and exact result for calculating the probability of error for two-dimensional signal constellations," in *Proc. IEEE MILCOM Conf. Rec.*, 1991, pp. 571–575.

[49] J. G. Proakis and M. Salehi, *Digital Communications*, vol. 4. New York, NY, USA: McGraw-Hill, 2001.

[50] K. Lu, S. Fu, Y. Qian, and H.-H. Chen, "SER performance analysis for physical layer network coding over AWGN channels," in *Proc. IEEE Glob. Telecommun. Conf. (GLOBECOM)*, 2009, pp. 1–6.

[51] V. Syrjala, M. Valkama, N. N. Tchamov, and J. Rinne, "Phase noise modeling and mitigation techniques in OFDM communications systems," in *Proc. IEEE Wireless Telecommun. Symp.*, 2009, pp. 1–7.

[52] J. Schmitz, F. Bartsch, M. Hernández, and R. Mathar, "Distributed software defined radio testbed for real-time emitter localization and tracking," in *Proc. IEEE Int. Conf. Commun. Workshops (ICC Workshops)*, 2017, pp. 1246–1252.

[53] D. Vasisht, S. Kumar, and D. Katabi, "Decimeter-level localization with a single WiFi access point," in *Proc. 13th USENIX Symp. Netw. Syst. Design Implement. (NSDI)*, 2016, pp. 165–178.
[54] E. Hamed, H. Rahul, M. A. Abdelghany, and D. Katabi, "Real-time distributed MIMO systems," in *Proc. ACM SIGCOMM Conf.*, 2016, pp. 412–425.
[55] R. Zhao *et al.*, "OFDMA-enabled Wi-Fi backscatter," in *Proc. 25th Annu. Int. Conf. Mobile Comput. Netw.*, 2019, pp. 1–15.
[56] M. Kotaru, K. Joshi, D. Bharadia, and S. Katti, "SpotFi: Decimeter level localization using WiFi," *ACM SIGCOMM Comput. Commun. Rev.*, vol. 45, no. 4, pp. 269–282, 2015.
[57] H. Meyr, M. Moeneclaey, and S. Fechtel, *Digital Communication Receivers: Synchronization, Channel Estimation, and Signal Processing*. Hoboken, NJ, USA: Wiley, 1997.
[58] M. R. Souryal, L. Klein-Berndt, L. E. Miller, and N. Moayeri, "Link assessment in an indoor 802.11 network," in *Proc. IEEE Wireless Commun. Netw. Conf. (WCNC)*, vol. 3, 2006, pp. 1402–1407.
[59] B. Bloessl, M. Segata, C. Sommer, and F. Dressler, "Performance assessment of IEEE 802.11p with an open source SDR-based prototype," *IEEE Trans. Mobile Comput.*, vol. 17, no. 5, pp. 1162–1175, May 2018.
[60] S. El Barrak, A. Lyhyaoui, A. Puliafito, and S. Serrano, "Implementation of a low cost SDR-based spectrum sensing prototype using USRP and Rasbperry Pi board," *Proc. Eng. Technol. PET*, vol. 20, pp. 54–58, Mar. 2017.
[61] R. Danymol, T. Ajitha, and R. Gandhiraj, "Real-time communication system design using RTL-SDR and Raspberry Pi," in *Proc. Int. Conf. Adv. Comput. Commun. Syst.*, 2013, pp. 1–5.
[62] C. Liu *et al.*, "RSS distribution-based passive localization and its application in sensor networks," *IEEE Trans. Wireless Commun.*, vol. 15, no. 4, pp. 2883–2895, Apr. 2016.
[63] D. Vasisht, A. Jain, C.-Y. Hsu, Z. Kabelac, and D. Katabi, "Duet: Estimating user position and identity in smart homes using intermittent and incomplete RF-data," in *Proc. ACM Interact. Mobile Wearable Ubiquitous Technol.*, vol. 2, 2018, p. 84.
[64] Y. Li and L. Cai, "Cooperative device-to-device communication for uplink transmission in cellular system," *IEEE Trans. Wireless Commun.*, vol. 17, no. 6, pp. 3903–3917, Jun. 2018.
[65] "Study on provision of low-cost machine-type communications (MTC) user equipments (UEs) based on LTE," 3rd Gener. Partnership Project, Sophia Antipolis, France, Rep. TR 36.888, 2013.
[66] S.-M. Oh and J. Shin, "An efficient small data transmission scheme in the 3GPP NB-IoT system," *IEEE Commun. Lett.*, vol. 21, no. 3, pp. 660–663, Mar. 2017.
[67] M. Shirvanimoghaddam, M. Dohler, and S. J. Johnson, "Massive non-orthogonal multiple access for cellular IoT: Potentials and limitations," *IEEE Commun. Mag.*, vol. 55, no. 9, pp. 55–61, Sep. 2017.
[68] B. Han *et al.*, "Maranello: Practical partial packet recovery for 802.11," in *Proc. NSDI*, 2010, pp. 205–218.
[69] K. C.-J. Lin, N. Kushman, and D. Katabi, "ZipTx: Harnessing partial packets in 802.11 networks," in *Proc. 14th ACM Int. Conf. Mobile Comput. Netw.*, 2008, pp. 351–362.
[70] H. Wu *et al.*, "The tick programmable low-latency SDR system," in *Proc. 23rd Annu. Int. Conf. Mobile Comput. Netw.*, 2017, pp. 101–113.

Wen Cui (Student Member, IEEE) received the B.S. degree in computer science from the Xi'an University of Science and Technology, Xi'an, China, in 2013, and the M.S. degree in software engineering from Northwest University, Xi'an, in 2016. He is currently pursuing the Ph.D. degree with the Department of Electrical and Computer Engineering, University of Victoria, Victoria, BC, Canada.

His research interests include wireless communication and Internet of Things.

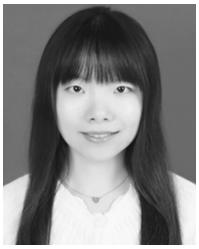

Chen Liu received the B.S., M.S., and Ph.D. degrees in computer science from Northwest University, Xi'an, China, in 2009, 2012, and 2016, respectively.

She is currently an Engineer with Northwest University and a Postdoctoral Research Fellow with the Department of Electrical and Computer Engineering, University of Victoria, Victoria, BC, Canada. Her research interests include wireless sensing, localization, and wireless networks.

Hamed Mosavat-Jahromi (Student Member, IEEE) received the B.Sc. degree in electrical engineering from the Iran University of Science and Technology, Tehran, Iran, in 2012, and the M.Sc. degree in electrical engineering from the University of Tehran, Tehran, in 2015. He is currently pursuing the Ph.D. degree in electrical engineering with the Department of Electrical and Computer Engineering, University of Victoria, Victoria, BC, Canada.

His research interests include vehicular networks, Internet of Things, machine learning, and optimization with applications in networking.

Lin Cai (Fellow, IEEE) received the M.A.Sc. and Ph.D. degrees in electrical and computer engineering from the University of Waterloo, Waterloo, ON, Canada, in 2002 and 2005, respectively.

Since 2005, she has been with the Department of Electrical and Computer Engineering, University of Victoria, Victoria, BC, Canada, where she is currently a Professor. She is an NSERC E.W.R. Steacie Memorial Fellow. Her research interests span several areas in communications and networking, with a focus on network protocol and architecture design supporting emerging multimedia traffic and the Internet of Things.

Prof. Cai was a recipient of the NSERC Discovery Accelerator Supplement Grants in 2010 and 2015, respectively, and the Best Paper Awards of IEEE ICC 2008 and IEEE WCNC 2011. She has founded and co-chaired the IEEE Victoria Section Vehicular Technology and Communications Joint Societies Chapter. She has been elected to serve the IEEE Vehicular Technology Society Board of Governors from 2019 to 2021. She has served as an Area Editor for the IEEE TRANSACTIONS ON VEHICULAR TECHNOLOGY, a member of the Steering Committee of the IEEE TRANSACTIONS ON BIG DATA and the IEEE TRANSACTIONS ON CLOUD COMPUTING, an Associate Editor of the IEEE INTERNET OF THINGS JOURNAL, the IEEE TRANSACTIONS ON WIRELESS COMMUNICATIONS, the IEEE TRANSACTIONS ON VEHICULAR TECHNOLOGY, the IEEE TRANSACTIONS ON COMMUNICATIONS, the *EURASIP Journal on Wireless Communications and Networking*, the *International Journal of Sensor Networks*, and the *Journal of Communications and Networks*, and as the Distinguished Lecturer of the IEEE VTS Society. She has served as a TPC Co-Chair for IEEE VTC2020-Fall, and a TPC Symposium Co-Chair for IEEE Globecom'10 and Globecom'13. She is a Registered Professional Engineer in British Columbia, Canada.